Statistical approach to systems engineering for the Thirty Meter Telescope

George Z. Angeli*, Konstantinos Vogiatzis
Thirty Meter Telescope Observatory, 1200 E. California Blvd. Mail Code 102-8, Pasadena, CA, USA 91125

ABSTRACT

Core components of systems engineering are the proper understanding of the top level system requirements, their allocation to the subsystems, and then the verification of the system built against these requirements. System performance, ultimately relevant to all three of these components, is inherently a statistical variable, depending on random processes influencing even the otherwise deterministic components of performance, through their input conditions. The paper outlines the Stochastic Framework facilitating both the definition and estimate of system performance in a consistent way. The environmental constraints at the site of the observatory are significant design drivers and can be derived from the Stochastic Framework, as well. The paper explains the control architecture capable of achieving the overall system performance as well as its allocation to subsystems. An accounting for the error and disturbance sources, as well as their dependence on environmental and operational parameters is included. The most current simulations results validating the architecture and providing early verification of the preliminary TMT design are also summarized.

Keywords: systems engineering, Thirty Meter Telescope, performance estimate, performance allocation, image quality, environmental conditions

1. INTRODUCTION

Core components of systems engineering are the proper understanding of the top level system requirements, their allocation - or flow down - to the subsystems, and then the verification of the design and the system built against these requirements. In earlier reports [1,2] we showed how TMT performance estimates, used for validating the requirements flow down as well as for early verification of the design, were formalized on statistical basis. The underlying concept was that system performance is inherently a statistical variable, depending on random processes influencing even the otherwise deterministic components of performance, through their input conditions. The logical extension of this concept is to define the requirements themselves in stochastic fashion.

TMT selected Mauna Kea as the preferred site for the observatory, which opened up the opportunity for further detailing the statistical framework of the "Standard Year" used in former analyzes. Three years of TMT site testing data [3] allowed us to extend the framework to three years from the single one originally considered. Furthermore, the observing sequences of Gemini now are for the same mountain and the same time period as the environmental sequences that lends the current TMT "Stochastic Framework" even more credibility. Using this framework is somewhat analogous to carrying out the thought experiment of replacing Gemini with TMT for 3 years, then defining and "measuring" its performance. Of course, the analogy is not perfect, as (i) Gemini is on the summit ridge, while the prospective TMT site is at 13N, and (ii) the actual Gemini observation sequence may be different from TMT sequences.

This paper focuses on the seeing limited performance of the observatory. The metric of this performance is the Normalized Point Source Sensitivity (PSS_N) defined and characterized elsewhere [4]. It relates the required science integration time of the actual observatory to that of the perfect telescope looking through the same atmosphere.

Section 2 summarizes the environmental and operational input parameters included in the Stochastic Framework, together with their key statistics. Section 3 briefly outlines the methodology used to derive the environmental constraint requirements for TMT and reports the resulting ranges. Section 4 presents the TMT image quality error budget and its dependence on the input parameters, while Section 5 summarizes the current performance estimate for TMT.

*gangeli@tmt.org; phone 1 520 318-8413; fax 1 520 318-8590; tmt.org

Modeling, Systems Engineering, and Project Management for Astronomy IV,
edited by George Z. Angeli, Philippe Dierickx, Proc. of SPIE Vol. 7738, 773817
© 2010 SPIE · CCC code: 0277-786X/10/$18 · doi: 10.1117/12.858245

2. STATISTICAL INPUT PARAMETERS

2.1 Environment

The environmental parameters considered for the Stochastic Framework are (i) external wind speed and (ii) direction, (iii) ambient temperature, and (iv) relative humidity outside of the enclosure. Data collected during the entire period of TMT site testing on Mauna Kea (from June 29th, 2005 to June 1st, 2008) was included in the Stochastic Framework, in order to account for as much seasonal and annual variations as possible. The site sunset and sunrise in Universal Time (UT) corresponding to the data records have also been incorporated.

The sampling rate of 2 minutes was chosen. While it was partially dictated by the availability of weather station and telescope orientation data, it is also equivalent to at least one flow-through time for the enclosure at 10 percentile external wind speeds, enough for the flow inside the enclosure to establish a large scale pattern. During that time the telescope-enclosure orientation can be considered fixed (maximum 0.5° change for tracking). Incidentally, the 2 minutes time period also enables the use of long exposure metrics, like the PSSN; furthermore, it is short enough to support the assumption of statistical independence among the environmental parameters. The various cross-couplings manifest themselves over significantly longer time periods and consequently are accounted for in the Stochastic Framework.

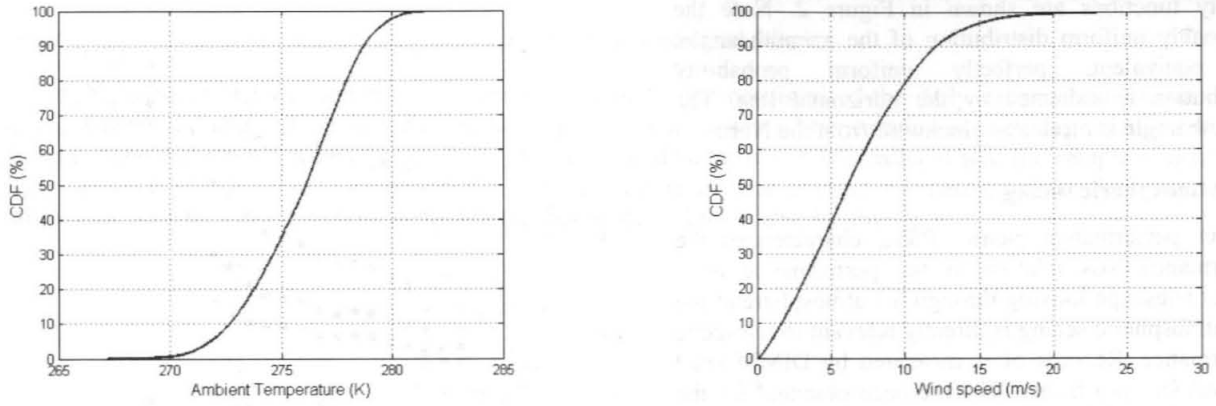

Figure 1 The night-time cumulative probability distribution of ambient temperature (left) and external wind speed (right) at 20 meters above ground (1 minute averages).

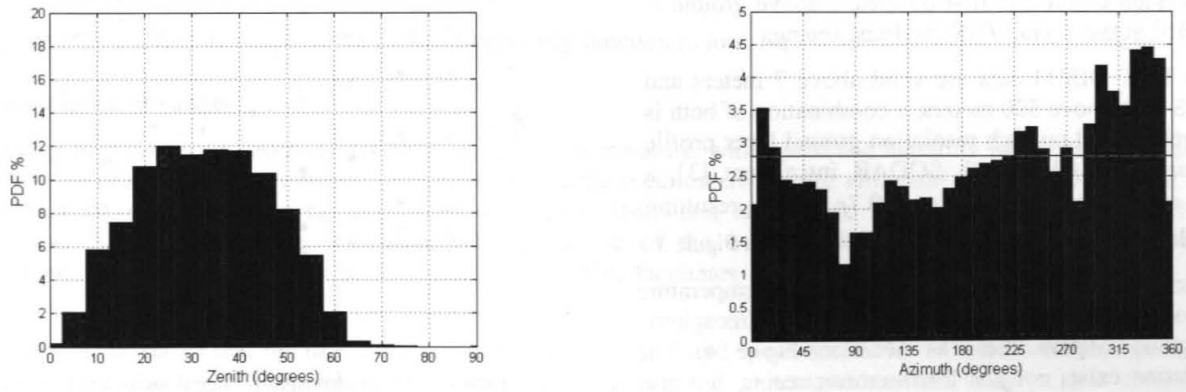

Figure 2 Telescope zenith (left) and azimuth (right) angles probability density distributions. For the azimuth angle distribution, the horizontal line indicates the equivalent uniform probability value

The average height of the enclosure vent locations is 20 meters above ground, designed to correspond to the position of M1. The night-time temperature and wind speed cumulative distributions at 20 meters are shown in Figure 1. The wind speed distribution was scaled from the actual data captured at 7 meters, based on 30 meters weather tower measurements at Cerro Armazones [3], adjusted to Mauna Kea conditions by CFD simulations; the scaling factor was 1.1.

2.2 Telescope orientation

A record of telescope azimuth and elevation angles has been obtained from the Gemini North Observatory [5], located on the summit ridge of Mauna Kea. The record is for the same time period (from June 29th, 2005 to June 1st, 2008) as the environmental data assembled for. The telescope zenith and azimuth angle probability density functions are shown in Figure 2. Note the reasonably uniform distribution of the azimuth angle; the equivalent, perfectly uniform probability distribution is indicated by the horizontal line. The azimuth angle is measured clockwise from the North.

2.3 Atmospheric seeing

As our performance metric, PSS_N, characterizes the performance loss relative to the performance of a perfect telescope looking through the atmosphere at the site, atmospheric seeing is directly relevant to telescope performance. Records of r_0 measured by DIMM (r_{0D}) and MASS (r_{0M}) from 13N have been obtained for the same period of time. The correct r_0 value required for evaluating PSS_N should exclude the first 60 meters, because of the enclosure influence. The seeing degradation due to the first 60 meters above ground is included in the overall PSS_N as dome seeing.

Since TMT DIMM data are valid above 7 meters and MASS data above 500 meters, a combination of both is required. Based on high resolution ground layer profile measurements taken with SODAR instrument [3], a good approximation is $0.3r_{0M} + 0.7r_{0D}$. The resulting cumulative probability distribution is shown in Figure 3.

Site testing data suggest that the ambient temperature and local wind speed are correlated with atmospheric seeing on Mauna Kea, as seen in Figure 4. The correlation exists not just for the mean seeing, but also for the best expected seeing.

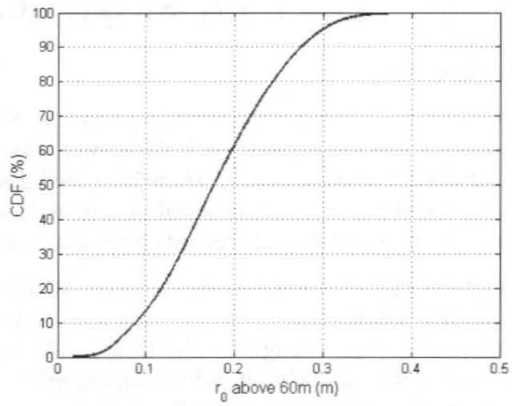

Figure 3 Cumulative probability distribution of atmospheric r_0 above 60 meters

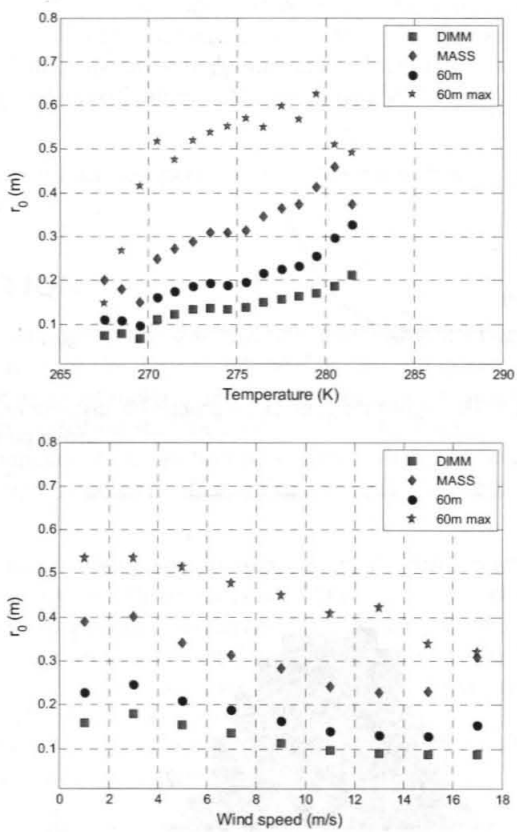

Figure 4 Mean atmospheric r_0 values as a function of ambient temperature and wind speed; the maximum expected values above 60 meters are also included

3. ENVIRONMENTAL DESIGN CONSTRAINTS

3.1 Methodology

Based on the 3 years record of environmental parameters, we can establish several levels of environmental constraints. For constraints with high probability, the joint environmental records in the Stochastic Framework can be used directly to define the appropriate parameter ranges. However, for very low probability, survival type conditions, the actual records need to be further processed. For these conditions, the "tails" of the probability density distribution are essential, while these are the most uncertain parts of any measured density function. In order to properly evaluate quartiles and return period events for a generally unbounded variable from a limited sample we first need to fit a smooth unbounded probability density function. We use the kernel density estimate (KDE) approach [6] with a Gaussian kernel and a bandwidth (standard deviation) optimized for Gaussian probability density functions. The estimated density at a given value x_k is then given by

$$f(x_k) = \frac{1}{nb}\sum_{i=1}^{n} K\left(\frac{x_k - x_i}{b}\right) \tag{1}$$

Where $K(z)$ is the normal probability density function with $\mu = 0$ and $\sigma = 1$, x_i are the sample values and $b = a\sigma_{sample} n^{-1/5}$. The constant '$a$' is very close to unity and is assumed 1 here.

For return period events we first use a subset of the sample that consisted of the daily extreme values (maxima or minima) for the variables of interest, for instance, the minimum observed temperature at each day through the whole database. Then we use the KDE approach with variable bandwidth, which is smaller where the sample is denser and larger where it is sparse (close to the boundaries). This technique requires an initial estimate f_{init} with a fixed bandwidth b as above and then the calculation of the final density estimate f with variable bandwidth as

$$\begin{aligned} f_e &= \left(\prod_{i=1}^{n} f_{init}(x_i)\right)^{1/n} \\ b_i &= \min\left\{ b\left(\frac{f_e}{f_{init}(x_i)}\right)^{1/2}, \sigma_{sample} \right\} \end{aligned} \tag{2}$$

The probability for a once in N-year event in a given variable, computed from a dataset of daily values, is $1/(365N)$. This probability is then matched in the probability density function to look for the absolute value of the variable.

3.2 Requirement ranges

Observing Performance Conditions define the ranges of temperature, wind speed and humidity where the observatory is expected to meet all the requirements. We chose to set the requirement for the *ensemble (long term) average* of the image quality over this entire range, instead of defining the worst case image quality to be met under all these conditions. While this average is a more relevant metric of the overall science capability of the observatory, understanding the actual statistics of the image quality also facilitates better insight into the technical trades of the design.

Conditions were set so that the total loss due to temperature and wind speed should be ~1% on combined probability distribution for the night. The ~1% of observing night-time lost due to temperature and wind is split: temperature accounts for 0.11% (0.1%-99.99%) and wind for 0.89% (0%-99.11%).The choice of including the 99.99% observing temperature limit is supported by the fact that seeing improves with increasing ambient temperature (see

Figure 4).

The resulting temperature range is [268.1, 282.3] (K), while the wind speed range is [0, 18.3] (m/s).

The intent of the *Facility Performance Conditions* is to describe the range of conditions over which all requirements relating to the enclosure and summit facilities are met as well as requirements relating to any other parts of the

observatory used for servicing or maintenance activities. While the enclosure may be open and observations may also be feasible under these conditions, overall system performance is not guaranteed. However, the enclosure is definitely expected to be closed when conditions are outside of Facility Performance ranges.

Since the external wind speed limit is related to structural operation and safety, rather than to image quality, the relevant metric is 3 seconds gust velocity and not 1 minute average. According to the ASCE 7-05 standard, the conversion factor from 1 minute average to 3 seconds gust is 1.25. By setting both the upper temperature and wind speed limits to the 99.9 percentile, they are 286 K and 30 m/s, respectively. For safety reasons, the lower temperature limit is set 5 K below the Observing Performance range.

Component Functional Conditions define the ranges over which any component of the system can be expected to function. Functioning does not imply that any system requirements are met over these ranges. The minimum temperature for the Component Functional conditions is selected to correspond to the expected minimum temperature that occurs once in any 10-year period (260 K). The maximum temperature is chosen to be the typical temperature expected in a laboratory environment (298 K). Wind is not relevant, as there is no level of system performance or safety associated with Component Functional Conditions.

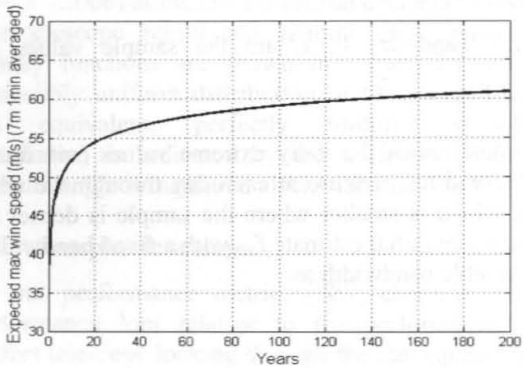

Figure 5 Return period events for maximum wind speed (1 minute average at 7 meters)

The observatory is designed to withstand the *Survival Conditions* without damage and without the need for optical realignment. Obviously, under these conditions the entire observatory is tightly closed. Similarly to the earthquake requirements, the environmental conditions are bounded by 200 year return period events. The probability for such an event to happen during the lifetime of the observatory (50 years) is 22%. The corresponding ranges are [256.9, 303.1] (K) for temperature and [0, 83.7] (m/s) for 3 seconds wind gust (60.9 m/s for 1 minute average at 7 meters).

3.3 Night-time temporal temperature gradients

Temporal temperature gradients are of particular importance for certain subsystem designs. The following Table 1 summarizes the gradients over the 3-year record for various integration times and quartiles. While the enclosure is designed to minimize the difference in thermal behavior of ambient and internal air, it has a low pass filtering effect, in particular below 1 minute integration time. However, the relevant integration time is defined by the thermal inertia, i.e. mass and size of a given subsystem, which is way above 1 minute for any practical cases for TMT.

Table 1 Night-time temporal temperature gradient ranges

Integration time (minutes)	min (K/h)	2.5% (K/h)	97.5% (K/h)	max (K/h)
1	-54.1	-9.4	9.4	57.0
4	-32.0	-5.5	5.3	30.9
8	-16.9	-3.4	3.2	13.5
16	-9.8	-2.2	2.0	7.2
32	-5.8	-1.5	1.2	3.7
60	-3.7	-1.1	0.7	2.1

4. OBSERVATORY PERFORMANCE ALLOCATION

The design of the observatory is constrained and defined by various requirements; outstanding among them are the optical performance requirements. Image size and image jitter is described by the Normalized Point Source Sensitivity (PSS_N). PSS_N is defined for on-axis and off-axis field points, as well as for various wavelengths and atmospheric conditions (r_0) [4,7]. Pupil stability is defined as the lateral stability of the first primary mirror (entrance pupil) image in the instrument. Plate scale stability is defined relative to the on-axis image point; it is the measure of the repeatability of the mapping of angles on the sky into positions on the focal surface. Telescope pointing accuracy, more precisely the telescope contribution to the pointing error is defined as the distance on the sky between the actual sky point the telescope settled on and the intended (theoretical) sky point.

The error budgets for telescope performance specify the *delivered* performance after active and/or adaptive optics wavefront correction. Therefore, the flow down of top level observatory requirements to the subsystem requirements and finally to the component specifications involves not only creating error budgets, but also defining the strategy and performance of the wavefront control systems supporting these budgets.

As the most developed example for our statistical approach, this paper focuses on the on-axis seeing limited image quality (size and jitter) budgets. The image quality of TMT is allowed to degrade by the factor 0.95 (5% loss) as the field position approaches the edge of the Field-of-View, 10 arcmin. By definition of the off-axis PSS_N, this degradation does not account for the inherent off-axis astigmatism of the optical design.

As it was mentioned earlier, performance statistics are specified and calculated for the Observing Performance Conditions.

4.1 Active optics wavefront control architecture

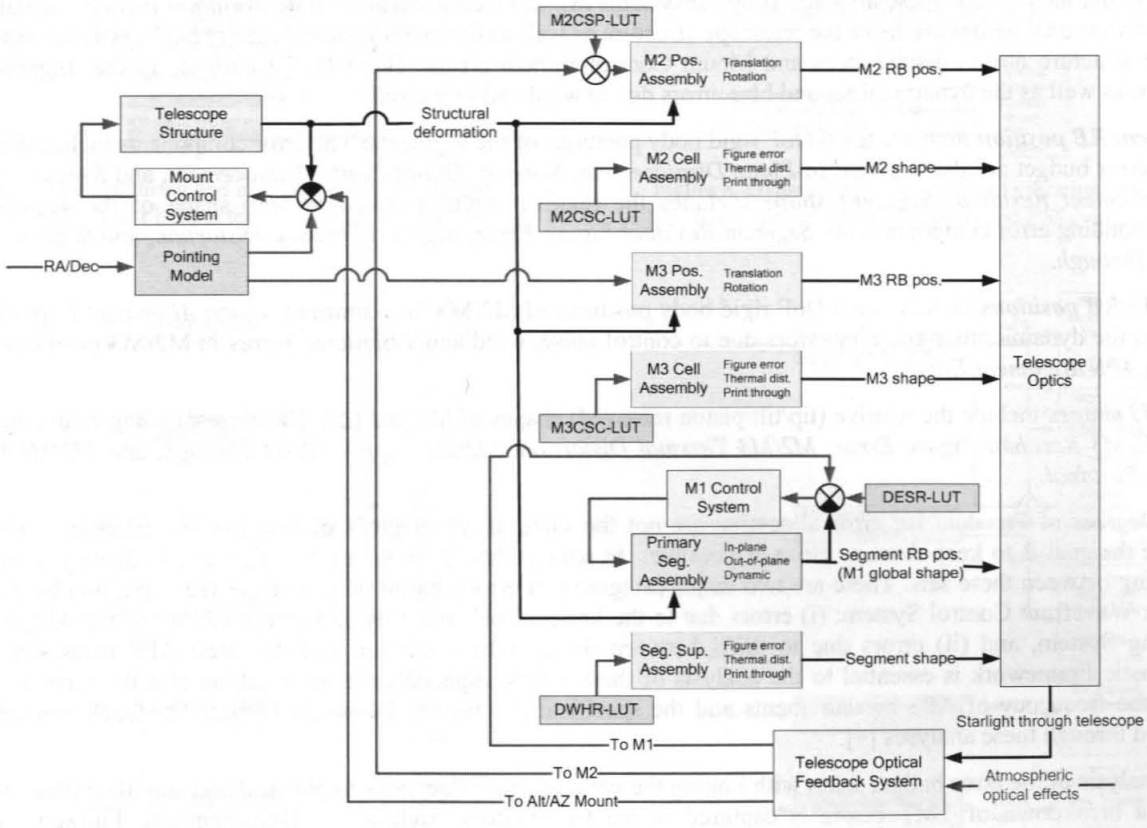

Figure 6 Top level control flow chart of the active optics wavefront control system (for abbreviations, see the text)

The wavefront control architecture of TMT is based on three layers of correction. At the first and innermost level, each of the controlled degrees of freedom are stabilized and stiffened by local control loops.

The optical alignment instrument, called the Alignment and Phasing System (APS), implements the middle layer of corrections. It uses starlight collected through the telescope to (i) phase the primary mirror segments, (ii) align the 3 mirrors of the telescope, (iii) optimize the global shape of M1, M2, and M3, and (iv) minimize segment shape errors. The optically optimized set points for each control loop are stored in Look-Up-Tables (LUT), as shown in Figure 6:

- M2 Positioner (M2CSP-LUT), controlling the rigid body position of M2;
- M2 Cell (M2CSC-LUT), controlling the shape of M2;
- M3 Cell (M3CSC-LUT), controlling the shape of M3
- Desired Edge Sensor Readout (DESR-LUT), controlling the phasing and global shape of M2;
- Desired Warping Harness Readout (DWHR-LUT), controlling the shape of the segments;
- The Pointing Model, controlling overall telescope pointing and the corresponding M3 rigid body position

The outermost control level utilizes real time optical loops to limit drifts in the active optics system and correct small errors not completely accounted for by the LUTs. In seeing limited observations (Figure 6), real time optical feedback is realized by the Telescope Optical Feedback System (TOFS) using wavefront sensors embedded in the seeing limited instruments. This extended guiding system feeds tip/tilt information to the alt/az drives (Mount Control System), while focus is corrected by M1-M2 separation, coma by M2 decenter, and higher order wavefront errors by M1 global shape. During diffraction limited observations, essentially the same optical feedback is provided by the AO System, in the form of deformable- and fast tip/tilt mirror off-loads (long term averages) to the telescope.

4.2 Image quality error budget

The TMT error budget primarily allocates image degradation to the various Degrees of Freedom (DoF) affecting image quality, and then groups these allocations by subsystems [8]. In Figure 6, ***Structural deformation*** includes actual thermal and gravitational deformations of the telescope structure as well as the overall, spatial mean pointing (direction) changes of the structure due to disturbances and Mount Control System errors. These DoF contribute to the *Alignment Drift Errors*, as well as the dynamic jitter and blur errors due to wind and vibrations.

Segment RB position includes the 6 DoF rigid body positions of the segments. The error components included in the top level error budget are the *Segment In-Plane Displacement*, *Segment Out-of-Plane Displacement*, and *Segment Dynamic Displacement Residual*. ***Segment shape*** includes the relative (tip/tilt/piston removed) shape of the segments. The corresponding error components are *Segment Residual Figure Error*, *Segment Thermal Distortion*, and *Segment Support Print Through*.

M2/M3 RB positions include the 6 DoF rigid body positions of M2/M3 that contribute to the *Alignment Drift Errors*, as well as the dynamic jitter and blur errors due to control noise, wind and vibrations. Errors in M2/M3 positions are also due to *APS Alignment Error*.

M2/M3 shapes include the relative (tip/tilt/piston removed) shapes of M2 and M3. The corresponding error components are *M2/M3 Residual Figure Error*, *M2/M3 Thermal Distortion*, *M2/M3 Support Print Through*, and *M2/M3 Dynamic Shape Residual*.

The Degrees of Freedom for error allocation are not the same as the Degrees of Freedom for actuation, although of course the goal is to keep them as close as possible. In reality, though, there are technical and budgetary limits on the mapping between these sets. There are two major categories of errors, based on their expected correction by the Active Optics Wavefront Control System: (i) errors due to the limits of observability and controllability of the Alignment and Phasing System, and (ii) errors due to drifts between the actual observation and the latest APS measurement. The Stochastic Framework is essential to the analysis of these errors, especially for those falling into the second category. Both the frequency of APS measurements and the specifications for the Telescope Optical Feedback System can be derived through these analyses [9].

The analysis of the error budget starts with linking the various error allocations to physical and manufacturing processes. Such a breakdown of TMT errors is captured in the Observatory Architecture Document [8]. Furthermore, these processes then can be linked to the underlying environmental and operational parameters of the Stochastic Framework and through these parameters the statistical nature of the top level performance requirement can be caught in the error budget. A visual representation of these dependencies is shown in Figure 7, Figure 8, and Figure 9.

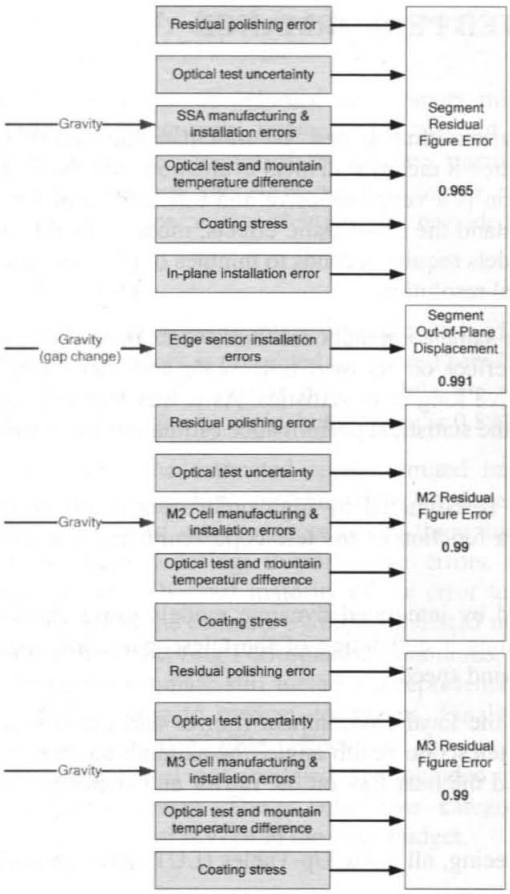

Figure 7 Manufacturing and installation effects and the associated error budget terms and PSS_N values

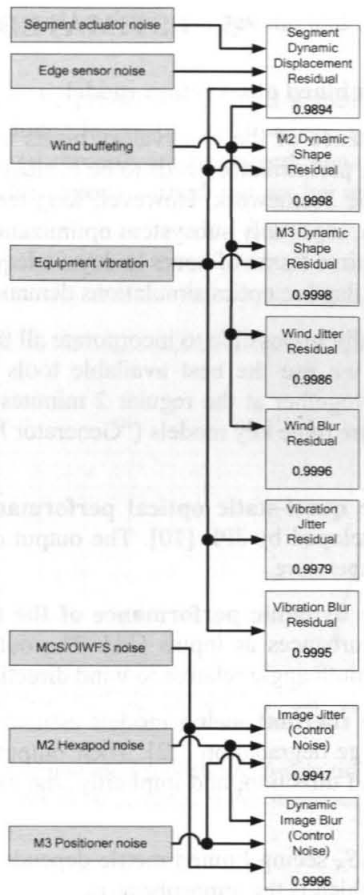

Figure 8 Dynamic effects (wind and vibration) and the associated error budget terms and PSS_N values

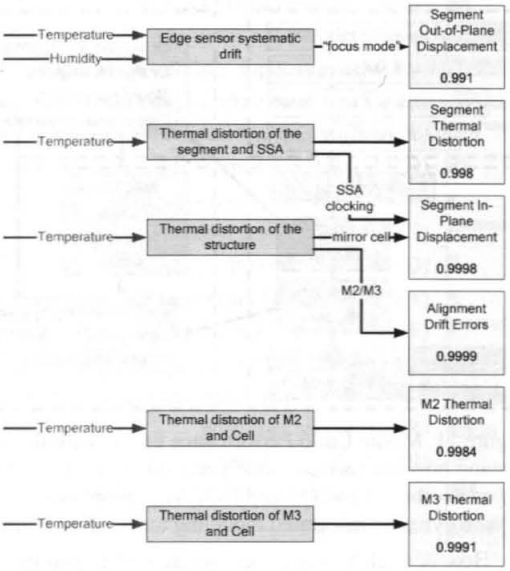

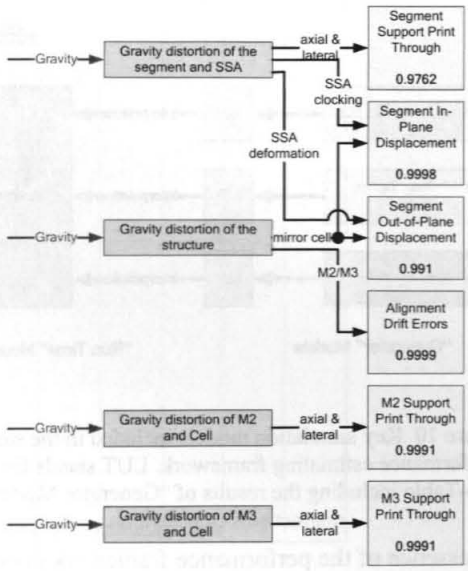

Figure 9 Quasi-static effects and the associated error budget terms and PSS_N values

5. ESTIMATED SEEING LIMITED PERFORMANCE

5.1 The combined observatory model

The performance of the observatory needs to be understood at various time scales. To anticipate the overall science productivity, performance needs to be evaluated over years; in practice it means statistical evaluation over the 3 years of the Stochastic Framework. However, long term statistical evaluation is a very expensive and inflexible tool for design optimization, especially subsystem optimization. In order to understand the quasi-static effects, models should simulate them on the time frame of hours to days; adequate fidelity wind models require seconds to minutes of physical time to be simulated. Adaptive optics simulations demand even higher temporal resolution.

It is technically impossible to incorporate all these time scales in the same computational framework. Instead of a unified framework, we use the best available tools to understand each effect on its own time scale and then "stitch" the information together at the regular 2 minutes sampling rate to derive long term statistics. As it was formerly reported [1,2], there are three key models ("Generator Models") included in the statistical performance estimating framework (see Figure 10):

- The **quasi-static optical performance of the telescope** is estimated by high order optical modeling tools developed by JPL [10]. The output of the simulations is a function of the telescope zenith angle and the M1 temperature.
- The **dynamic performance of the telescope** is evaluated by integrated dynamic models using standardized disturbances as inputs [11]. The output of these simulations is a function of the telescope zenith angle, the azimuth angle relative to wind direction, and the external wind speed.
- The **thermal seeing** models estimate the contribution of the local environment (mirror and dome seeing) to image degradation [12]. Their output is a function of the telescope zenith angle, the azimuth angle relative to wind direction, and implicitly, the external wind speed and the heat flux on the mirror and enclosure surfaces [13].

Since the PSS_N seeing limited metric depends on the atmospheric seeing, all Look-Up-Tables (LUT) have an additional dimension which is the atmospheric r_0.

Additional models provide input to the framework or the above models. They include CFD simulations of the observatory on the TMT site [12], the radiation-convection enclosure skin temperature model, and the solid thermal models of the optical elements [14], their support structure and the telescope structure [15].

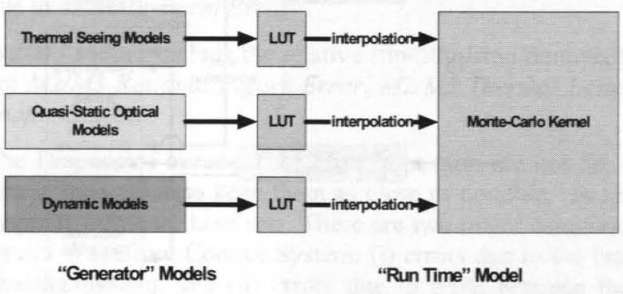

Figure 10 Key simulation models included in the stochastic performance estimating framework. LUT stands for Look-Up-Table including the results of "Generator Models" for distinct sets of conditions.

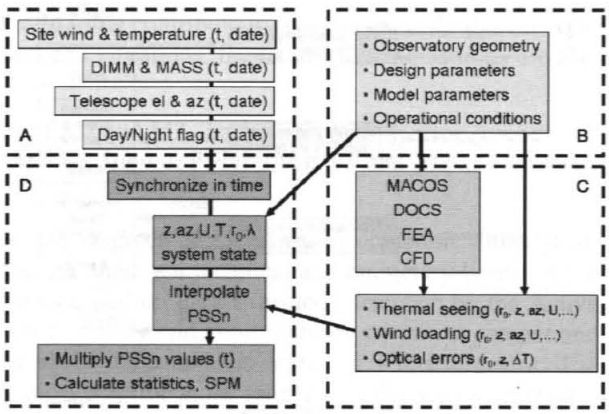

Figure 11 Monte Carlo Performance Framework flow-chart showing how the various models rely on inputs and the results of each other. (MACOS and DOCS are proprietary optical and dynamic integrated modeling tools, respectively.)

The essence of the performance framework is depicted in Figure 11. Box A (yellow) denotes the available inputs. Inside box B (cyan) is what can be controlled by design and operation. Box C (green) shows the developed models with pre-calculated aberrations in multidimensional matrix (LUT) form, spanning the range of all influencing parameters

(dimensions). Finally, functions in box D (purple) correspond to mathematical/statistical processing and are in fact the core of the time domain simulation.

In earlier simulations we assumed that primary mirror temperature cannot be properly estimated without knowing its time history. Consequently, mirror seeing was not parameterized and included in the LUTs. However, while it is true that at least the temperature of the primary mirror should also be tracked throughout the record, segment temporal thermal behavior and the corresponding mirror seeing and optical deformations turned out to be monotonic and predictable. Thus now mirror seeing is also provided in LUT form.

5.2 Performance

The cumulative probability distribution function of the estimated TMT errors is presented in Figure 12 in PSS_N metric. The expected value is 0.917, while the total error budget allocation to the included terms is 0.883.

Figure 13 shows the estimated seeing limited image quality of the observatory, in comparison to the error budget. The errors can be grouped in three major categories: thermal seeing, mirror shape errors, and alignment errors. The vast majority of the error terms are represented in the estimate by their simulated mean value over the Observing Performance Conditions. For some terms the estimate still includes a representative value corresponding to median conditions. Finally, a few terms with negligible effect on the overall performance are still not modeled but included with their budgeted values. These latter two categories account for a PSS_N of 0.9774 in the error budget.

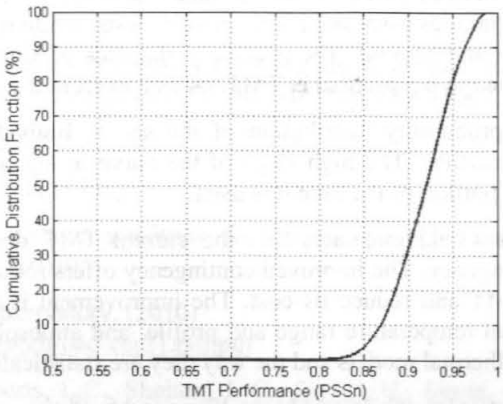

Figure 12 Cumulative probability distribution of the image quality error terms included in the Stochastic Framework.

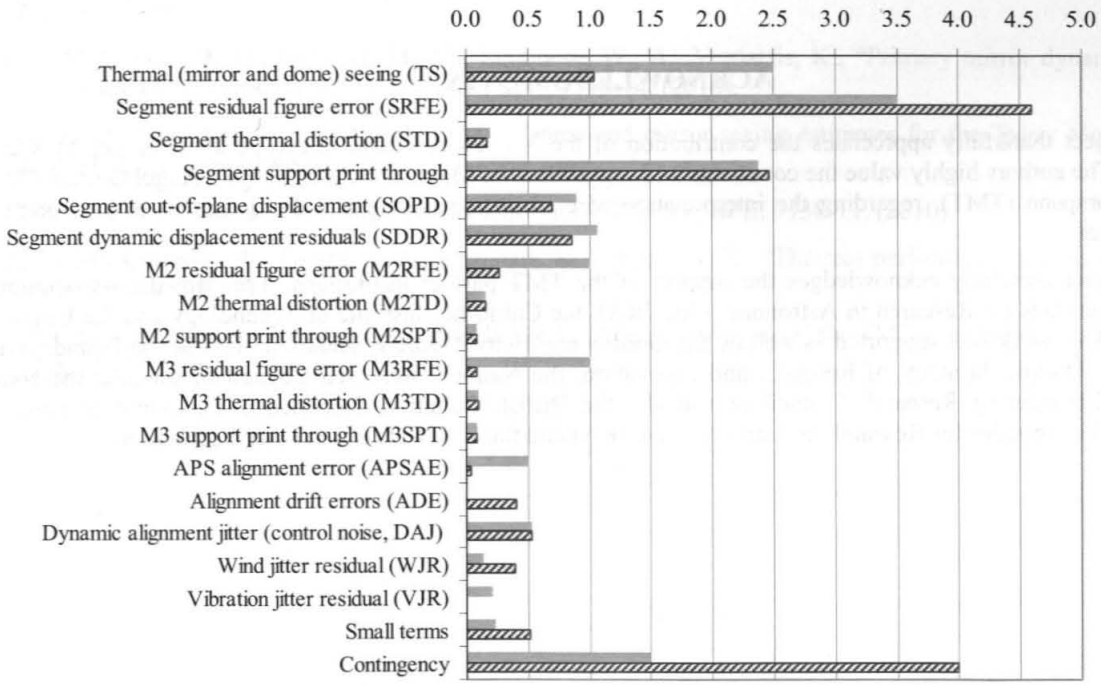

Figure 13 TMT performance estimate compared to the error budget (solid blue), expressed in (1-PSSN)%

6. CONCLUSION

A Stochastic Framework was developed to aid core systems engineering processes. The Framework is a useful tool, supporting a performance requirement definition that's relevant to the long term science capabilities of the observatory. It has also been applied in the performance allocation process. Being an extension to the Standard Year formerly developed for integrating the various system models, it is instrumental for the bottom-up performance estimates validating the Active Optics Wavefront Control Architecture and providing an early verification of the observatory design.

The statistical definition of seeing limited image quality enables robust verification by comparing the required statistics to measured ones, based on data collected over an extended time period. The process significantly reduces the uncertainties associated with singular tests, while it directly exploits data expected to be collected in the commissioning phase and beyond. The necessary statistics of atmospheric seeing can be derived from the MASS/DIMM instruments planned to be installed at TMT, as well as from the analysis of AO data.

The probability distribution of the seeing limited image quality indicates a "graceful degradation" of observatory performance. The high slope of the curve in Figure 12 reveals that the observatory performance is fairly stable over a large portion of the time it is used.

Figure 13 demonstrates that the current TMT design is expected to meet image quality requirements with ~25% contingency. The improved contingency offers robust support to the trade studies expected to further advance the design of TMT and reduce its cost. The improvement is the manifestation of a combination of factors: the air flow pattern, diurnal temperature range and profile, and atmospheric seeing on Mauna Kea, as well as advances in our optical and aero-thermal models and the way they are statistically combined.

In particular, while on Mauna Kea wind buffeting of the telescope structure is noticeably worse than expected, its effect is more than balanced by the better than expected dome and mirror seeing. The other noticeable discrepancy in Figure 13 is the worse than expected optical effect due to segment residual figure errors. However, current simulations reflect the nominal technology; some segment manufacturing and finishing procedures considered support definitely better performance.

ACKNOWLEDGMENTS

The TMT Project thankfully appreciates the contribution of the 3 years record of telescope alt/az angles by Gemini Observatory. The authors highly value the comments and suggestions of Matthias Schöck (TMT), Angel Otarola (TMT), and Hugh Thompson (TMT), regarding the interpretation of environmental data and the definition of environmental constraint ranges.

The TMT Project gratefully acknowledges the support of the TMT partner institutions. They are the Association of Canadian Universities for Research in Astronomy (ACURA), the California Institute of Technology and the University of California. This work was supported as well by the Gordon and Betty Moore Foundation, the Canada Foundation for Innovation, the Ontario Ministry of Research and Innovation, the National Research Council of Canada, the Natural Sciences and Engineering Research Council of Canada, the British Columbia Knowledge Development Fund, the Association of Universities for Research in Astronomy (AURA) and the U.S. National Science Foundation.

REFERENCES

[1] Angeli, G. Z., Roberts, S., and Vogiatzis, K., "Systems Engineering for the Preliminary Design of the Thirty Meter Telescope", Proc. SPIE 7017-03, (2008).

[2] Vogiatzis, K., and Angeli, G. Z., "Monte Carlo simulation framework for TMT", Proc. SPIE 7017-29, (2008).

[3] Schöck, M., Els, S., Riddle, R., Skidmore, W., Travouillon, T., Blum, R., Bustos, E., Chanan, G., Djorgovski, S. G., Gillett, P., Gregory, B., Nelson, J., Otárola, A., Seguel, J., Vasquez, J., Walker, A., Walker, D., Wang, L., "Thirty Meter Telescope Site Testing I: Overview," Publications of the Astronomical Society of the Pacific, Volume 121, issue 878, pp.384-395, (2009).

[4] Seo, B.-J., Nissly, C., Angeli, G. Z., Ellerbroek, B., Nelson, J., Sigrist, N., Troy, M., "Analysis of normalized point source sensitivity as a performance metric for large telescopes", Applied Optics, Vol.48, No.31, pp5997-6007, 2009.

[5] Mike Sheehan, Gemini Observatory, personal communication, 2010.

[6] Silverman, B., W., [Density Estimation], Chapman & Hall, London, (1986).

[7] Seo, B.-J., Nissly, C., Troy, M., Angeli, G. Z., "Normalized point source sensitivity for off-axis optical performance evaluation of the Thirty Meter Telescope," Proc. SPIE 7738-16, (2010).

[8] Observatory Architecture Document, Thirty Meter Telescope Observatory, (2010) http://www.tmt.org/sites/default/files/documents/application/pdf/oad-ccr21.pdf.pdf

[9] Nissly, C., Seo, B.-J., Troy, M., Angeli, G. Z., Cho, M., Roberts, L.C., Shelton, J. C., Sigrist, N., Sirota, M. J., "Investigation of Thirty Meter Telescope wavefront maintenance using low-order Shack-Hartmann wavefront sensors to correct for thermally induced misalignment", Proc. SPIE 7738-17, (2010).

[10] Nissly, C., Seo, B.-J., Troy, M., Angeli, G. Z., Angione, J., Crossfield, I., Ellerbroek, B., Gilles, L., and Sigrist, N., "High-resolution optical modeling of the Thirty Meter Telescope for systematic performance trades", Proc. SPIE 7017-30, (2008).

[11] MacMynowski, D., G., Colavita, M., M., Skidmore, W., A., Vogiatzis, K., "Primary mirror dynamic disturbance models for TMT: vibration and wind", Proc. SPIE 7738-14, (2010).

[12] Pazder, J., Vogiatzis, K., and Angeli, G. Z., "Dome and mirror seeing estimates for the Thirty Meter Telescope", Proc. SPIE 7017-26, (2008).

[13] Vogiatzis, K., "Thermal modeling environment for TMT", Proc. SPIE 7738-11, (2010).

[14] Cho, M., Corredor, A., Pootrakul, S., Vogiatzis, K., Angeli, G. Z., "Thermal performance prediction of the TMT optics", Proc. SPIE 7017-43, (2008).

[15] Cho, M., Corredor, A., Vogiatzis, K., Angeli, G. Z., "Thermal analysis of the TMT telescope structure", Proc. SPIE 7738-12, (2010).